

# Chiral ground-state currents of interacting photons in a synthetic magnetic field

P. Roushan<sup>1\*†</sup>, C. Neill<sup>2†</sup>, A. Megrant<sup>1†</sup>, Y. Chen<sup>1</sup>, R. Babbush<sup>3</sup>, R. Barends<sup>1</sup>, B. Campbell<sup>2</sup>, Z. Chen<sup>2</sup>, B. Chiaro<sup>2</sup>, A. Dunsworth<sup>2</sup>, A. Fowler<sup>1</sup>, E. Jeffrey<sup>1</sup>, J. Kelly<sup>1</sup>, E. Lucero<sup>1</sup>, J. Mutus<sup>1</sup>, P. J. J. O'Malley<sup>2</sup>, M. Neeley<sup>1</sup>, C. Quintana<sup>2</sup>, D. Sank<sup>1</sup>, A. Vainsencher<sup>2</sup>, J. Wenner<sup>2</sup>, T. White<sup>1</sup>, E. Kapit<sup>4,5</sup>, H. Neven<sup>3</sup> and J. Martinis<sup>1,2</sup>

**The intriguing many-body phases of quantum matter arise from the interplay of particle interactions, spatial symmetries, and external fields. Generating these phases in an engineered system could provide deeper insight into their nature. Using superconducting qubits, we simultaneously realize synthetic magnetic fields and strong particle interactions, which are among the essential elements for studying quantum magnetism and fractional quantum Hall phenomena. The artificial magnetic fields are synthesized by sinusoidally modulating the qubit couplings. In a closed loop formed by the three qubits, we observe the directional circulation of photons, a signature of broken time-reversal symmetry. We demonstrate strong interactions through the creation of photon vacancies, or 'holes', which circulate in the opposite direction. The combination of these key elements results in chiral ground-state currents. Our work introduces an experimental platform for engineering quantum phases of strongly interacting photons.**

It is commonly observed that when the number of particles in a system increases, complex phases can emerge which were absent in the system when it had fewer particles, that is, the 'more is different'<sup>1</sup>. This observation drives experimental efforts in synthetic quantum systems, where the primary goal is to engineer and utilize these emerging phases. However, it has generally been overlooked that these sought-after phases can emerge only from simultaneous realization and control of particle numbers, real-space arrangements, external fields, particle interactions, state preparation, and quantum measurement. The simultaneous realization of all these ingredients makes synthesizing many-body phases a holistic task, and hence constitutes a major experimental challenge. Engineering these factors, in particular synthesizing magnetic fields, has been performed in several platforms<sup>2–12</sup>. However, these ingredients have not been jointly realized in any system thus far. To provide a tangible framework, we discuss realization of these key elements in the context of quantum Hall physics<sup>13,14</sup>, and show when these ingredients come together they can construct a basic building block for creating fractional quantum Hall (FQH) states.

The FQH states are commonly studied in two-dimensional electron gases, a fermionic condensed matter system<sup>13,14</sup>. However, many of the recent advancements in engineered quantum systems are taking place in bosonic platforms<sup>2,15–19</sup>. Theoretical studies suggest the existence of rich phases for bosonic FQH systems, similar to their fermionic counterparts<sup>20–25</sup>. In particular, bosonic FQH states are known to host non-Abelian anyons, which could implement quantum logic operations through braiding<sup>26</sup>. Among the prerequisites for realizing bosonic FQH states are: strong artificial gauge fields, leading to nearly flat single-particle bands; strong interactions; low disorder; and a mechanism for accessing the many-body ground state. In this work, we engineer a modular unit

cell consisting of three coupled qubits in a ring, which when tiled can be used to realize FQH phases (Fig. 1a,b)<sup>27,28</sup>. At low (uniform) flux densities, the single-particle band is nearly flat in this triangular configuration. However, we note that to obtain a denser FQH states, hopping beyond nearest neighbours is generally required to ensure band flatness. We concurrently demonstrate tunable gauge fields, strong interactions, and adiabatic ground-state preparation in a platform with low loss and disorder, where we have full state preparation and quantum correlation measurement capabilities.

## Synthetic gauge fields

When electrons hop between lattice sites of a crystal placed in a magnetic field, the wavefunction accumulates a path-dependent phase. The interference of electrons travelling along different paths is the fundamental origin of many rich many-body phases seen in correlated systems. However, due to the charge neutrality of photons, they are not affected by physical magnetic fields; therefore, an effective magnetic field has to be synthesized for quantum platforms with bosonic excitations<sup>2–6,29–32</sup>. One practical idea, proposed in various settings, suggests that artificial magnetic fields can be created by periodic modulation of the photon hopping strength between the lattice sites<sup>24,33,34</sup>. When the on-site energies of two lattice sites differ by  $\Delta$ , then sinusoidal modulation of a tunnelling term with frequency  $\Delta$  and phase  $\varphi$  results in an effective complex hopping, where the photon's wavefunction picks up phase  $\varphi$  (Fig. 1c). This phase is analogous to the Peierls phase  $e \oint \mathbf{A} \cdot d\mathbf{r}$  that is accumulated by a particle of charge  $e$  tunnelling in an external magnetic vector potential  $\mathbf{A}$ . This idea can be implemented in a superconducting qubit platform, where qubits play the role of the lattice sites, and modulating the strength of the inter-qubit couplings  $g$  sets the microwave photon hopping rate.

<sup>1</sup>Google Inc., Santa Barbara, California 93117, USA. <sup>2</sup>Department of Physics, University of California, Santa Barbara, California 93106, USA. <sup>3</sup>Google Inc., Los Angeles, California 90291, USA. <sup>4</sup>The Graduate Center, CUNY, New York, New York 10016, USA. <sup>5</sup>Department of Physics, Tulane University, New Orleans, Louisiana 70118, USA. <sup>†</sup>These authors contributed equally to this work. \*e-mail: [pedramr@google.com](mailto:pedramr@google.com)

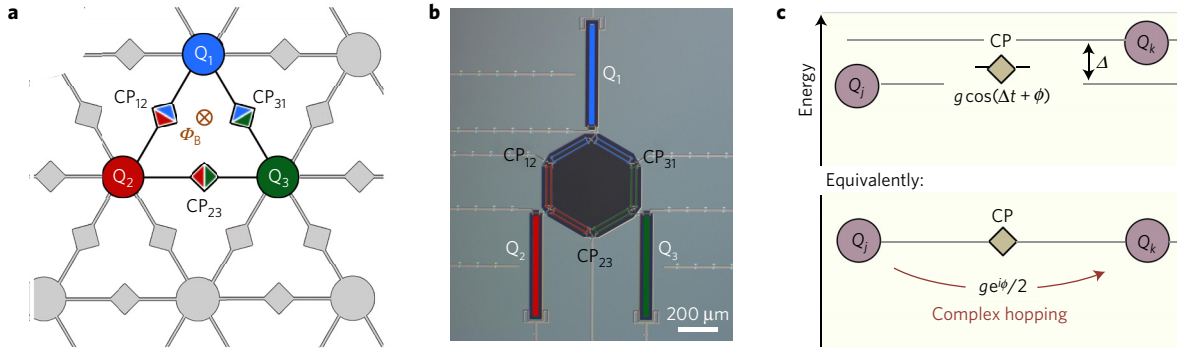


**Figure 1 | The unit cell for FQH and synthesizing magnetic fields. a**, A schematic illustration of how qubits and their couplers can be tiled to create a two-dimensional lattice. The 3-qubit unit cell of this lattice, which is realized in this work, is highlighted. **b**, An optical image of the superconducting circuit made by standard nano-fabrication techniques. It consists of three superconducting qubits  $Q_j$  connected via adjustable couplers  $CP_{jk}$ . Together, they form a triangular closed loop. **c**, A parametric modulation approach is used for synthesizing magnetic fields. If the frequency difference of two qubits is  $\Delta$ , then the sinusoidal modulation of the coupler connecting them with frequency  $\Delta$  and phase  $\phi$  results in an effective resonance hopping ( $\Delta = 0$ ) with a complex hopping amplitude between the two qubits.

We place three transmon superconducting qubits in a ring (Fig. 1b), where each qubit is coupled to its neighbours via an adjustable coupler that can be dynamically modulated on nanosecond timescales<sup>35</sup>. The Hamiltonian of the system is

$$H(t) = \hbar \sum_{j=1}^3 \omega_j (\hat{n}_j + 1/2) + \hbar \sum_{j,k} g_{jk}(t) (a_j^\dagger a_k + a_j a_k^\dagger) + H_{\text{int}} \quad (1)$$

where  $a^\dagger$  ( $a$ ) are bosonic creation (annihilation) operators,  $\omega_j$  is frequency of qubit  $Q_j$ ,  $\hat{n} = a_j^\dagger a_j$  is the particle number operator, and  $g_{jk}$  is the strength of the inter-qubit coupling between qubits  $Q_j$  and  $Q_k$ .  $H_{\text{int}}$  captures the interaction between bosons and is set by the nonlinearity of the qubits. This term does not affect the dynamics in the single-photon manifold, and we will discuss its role in the two-photon manifold in more detail later. We modulate  $g$  of each coupler according to  $g_{jk}(t) = g_0 \cos(\Delta_{jk}t + \varphi_{jk})$ , and choose  $\Delta_{jk}$  to be the difference between the frequencies of the two qubits that the coupler connects, that is,  $\Delta_{jk} = \omega_j - \omega_k$  (Fig. 2b). If  $|g_{jk}| \ll |\omega_j - \omega_k|$ , then, in the rotating frame, the effective Hamiltonian of the system becomes

$$H_{\text{eff}}(\Phi_B) = \frac{\hbar}{2} \sum_{j,k} g_0 (e^{i\varphi_{jk}} a_j^\dagger a_k + e^{-i\varphi_{jk}} a_j a_k^\dagger) \quad (2)$$

where  $\Phi_B \equiv \varphi_{12} + \varphi_{23} + \varphi_{31}$  is the effective magnetic flux and is gauge-invariant. One can intuitively understand the origin of the gauge invariance of  $\Phi_B$  by noting that the three qubits in our case form a closed loop, and the accumulated phase needs to be single-valued when going around this loop. In other words, if the qubits' loop were open,  $\Phi_B$  would not be gauge-invariant (see Supplementary Information for details).

### Single-photon circulation

Based on this idea, we construct a protocol (Fig. 2b) and study the dynamics of single microwave photons in our system. At  $t = 0$ , we create a microwave photon which occupies  $Q_1$  ( $\psi_0 = |100\rangle$ ), and measure  $P_{Q_j}$ , the photon occupation probability of  $Q_j$ , as a function of time. As shown in the middle panel of Fig. 2c, the photon has a symmetric evolution for  $\Phi_B = 0$ . It propagates from  $Q_1$  to  $Q_3$  and  $Q_2$  simultaneously, then back to  $Q_1$ , and then repeats the pattern with no indication of any preferred circulation direction (blue  $\rightarrow$  red  $\rightarrow$  green  $\rightarrow$  blue  $\rightarrow$  ...). Setting  $\Phi_B = \pi/2$  leads to fundamentally different dynamics, where the photon propagation shows a preferred circulation direction and marches in a clockwise order from  $Q_1$ , to  $Q_3$ , to  $Q_2$ , eventually back to  $Q_1$ , and then repeating the pattern (blue  $\rightarrow$  green  $\rightarrow$  red  $\rightarrow$  blue  $\rightarrow$  ...). Choosing

$\Phi_B = -\pi/2$  leads to anticlockwise circulation, demonstrating that the synthetic flux  $\Phi_B$  behaves fairly similarly to physical magnetic flux.

The hallmark of magnetic fields in a system is the breaking of time-reversal symmetry (TRS). Commonly, TRS preserving evolution of the state is defined as  $\psi(t) = \psi(-t)$ . Verifying TRS breaking based on this relation in a real experiment can be difficult, since reversing the flow of time is generally not feasible. However, the dynamics considered here is periodic with period  $T = 280$  ns for  $\Phi_B = \pm\pi/2$  and  $T = 170$  ns for  $\Phi_B = 0$  case. This periodicity allows us to arrive at a practical definition for TRS, which is  $\psi(t) = \psi(T - t)$ ; for example, one could follow the evolution of state from  $t = T$  backwards and see if it is the same as going forwards from  $t = 0$ . It can be seen in Fig. 2c that TRS is preserved for  $\Phi_B = 0$  and is broken when  $\Phi_B = \pm\pi/2$ . These observations establish TRS breaking for  $\Phi_B = \pm\pi/2$  and further illustrate that the synthetic flux  $\Phi_B$  indeed behaves akin to physical magnetic flux. The quantum nature of the circulation is manifested through quantum correlation measurements which show entanglement between qubits (see Supplementary Information for data). The measured entanglement makes our experiment distinct from others which are based on classical wave mechanics or those where the timescales are much longer than the quantum coherence of the system—that is, are in the semi-classical limit<sup>7-11,33,36-41</sup>.

### Strongly interacting photons

We next focus on signatures of strong interactions, which are vital for realizing FQH states, as the many-body gap is set by the smaller of  $g$  and  $U$ . The typical weakness of interactions between bosons makes studying many-body quantum phenomena a major engineering challenge<sup>20</sup>. Superconducting qubits, however, naturally overcome this challenge and provide a platform where microwave photons can have strong interactions. Systems of coupled qubits can be understood with a Bose-Hubbard model, where the on-site interaction  $U$  originates from the expansion of the qubit's confining cosine potential:

$$H_{\text{int}} = -\frac{U_2}{2} \sum_j \hat{n}_j (\hat{n}_j - 1) + \frac{U_3}{6} \sum_j \hat{n}_j (\hat{n}_j - 1) (\hat{n}_j - 2) + \dots \quad (3)$$

In our system  $U_2 \approx U_3 \sim 200$  MHz, which sets the energy difference between single- and double-photon occupancy; for example, the  $|200\rangle$  to  $|110\rangle$  transition. The hopping 'bandwidth' in each manifold is set by  $g$  and is a few megahertz. Therefore  $U \gg g$ , and qubits effectively form a hard core boson system.

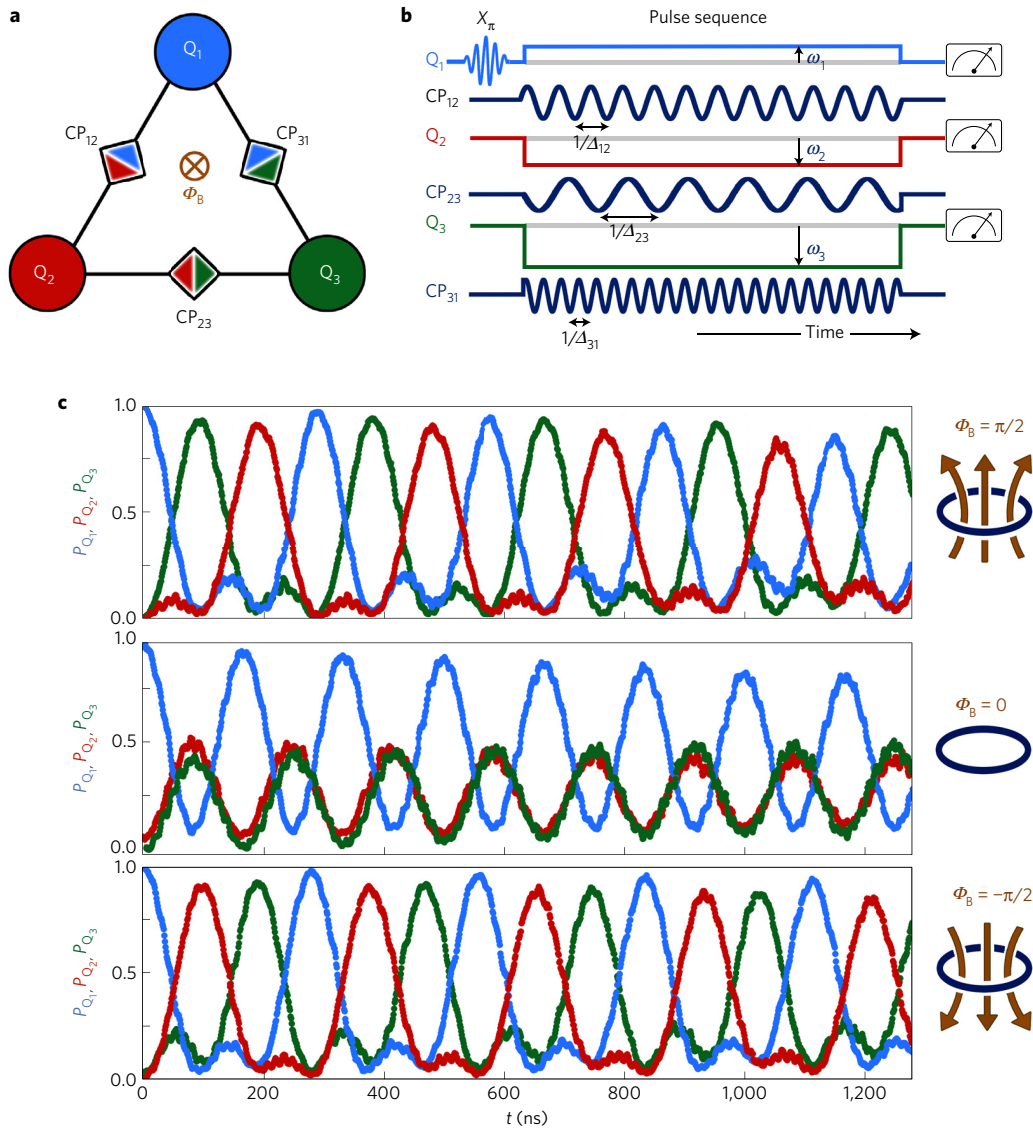


**Figure 2 | Single-photon circulation resulting from the TRS breaking.** **a**, Schematic of the three qubits and their couplers placed in a triangular closed loop. **b**, The pulse sequence used for generating and circulating a microwave photon shows that the qubits' frequencies  $\omega_j$  can be chosen to have arbitrary values, but each coupler needs to modulate with frequency  $\Delta_{jk}$ , set to the difference in the qubit frequencies that it connects  $\omega_j - \omega_k$ . The periodic modulation of each coupler can also have a phase  $\varphi_{jk}$ , where  $\Phi_B \equiv \varphi_{12} + \varphi_{23} + \varphi_{31}$ . **c**, A microwave photon is created by applying a  $\pi$ -pulse to  $Q_1$ , at  $t=0$  ( $|\psi_0\rangle = |100\rangle$ ). While applying the pulse sequence shown in **b**, the probability of a photon occupying each qubit  $P_{Q_i}$  as a function of time is measured for three values of  $\Phi_B = \pi/2, 0, -\pi/2$ . We use  $g_0 = 4$  MHz,  $\omega_1 = 5.8$  GHz,  $\omega_2 = 5.8$  GHz,  $\omega_3 = 5.835$  GHz,  $\Delta_{12} = 0$ ,  $\Delta_{23} = 35$  MHz,  $\Delta_{31} = 35$  MHz,  $\varphi_{12} = 0$ ,  $\varphi_{23} = 0$ , and  $\varphi_{31}$  was used to set  $\Phi_B$ .

The signature of strong interactions can be seen in the two-photon circulation as shown in Fig. 3b. In the absence of interactions one expects that two photons will circulate freely with the same chirality as a single photon. However, two-photon circulation in our system exhibits the opposite chirality, indicating that, as a result of strong interactions, photons do not move freely. Consequently, given that our system has three sites, when two photons are injected it is more natural to consider the motion of the photon-vacancy. Similar to the physics of holes in an electron band, the photon-vacancies have the opposite 'charge', and hence circulate in the opposite direction compared to photons.

### Chiral ground states

In condensed matter systems, one is generally interested in finding the ground state of a many-body system and probing its properties. In particular, the key signature of FQH states is the appearance of ground-state chiral edge currents. As the many-body Chern

number of FQH phases can be extracted from the d.c. conductivity tensor, the capability to measure ground-state currents is especially valuable. Although the evolution of  $|100\rangle$  or  $|110\rangle$ , as discussed so far, provides an intuitive understanding of the response of the system to this synthetic gauge, these data do not directly reflect the ground-state properties of the system, because these initial states are not eigenstates of the Hamiltonian. To study ground-state properties, we adiabatically prepare ground states of equation (2) and examine breaking the TRS by measuring the chiral current in the ground states (see Fig. 4a for pulse sequence). Analogous to the continuity equation in classical systems, a current operator  $\hat{I}$  can be defined by equating the current in and out of a qubit site to the change of the photon number operator on that site ( $\hat{I}_{\text{in}} - \hat{I}_{\text{out}} = d\hat{n}/dt$ ). From the continuity equations, we define the chiral current operator to be

$$\hat{I}_{\text{chiral}} \equiv \sum_{j,k} \hat{I}_{Q_j \rightarrow Q_k} = i \sum_{j,k} (e^{i\varphi_{jk}} a_j^\dagger a_k - e^{-i\varphi_{jk}} a_j a_k^\dagger) \quad (4)$$

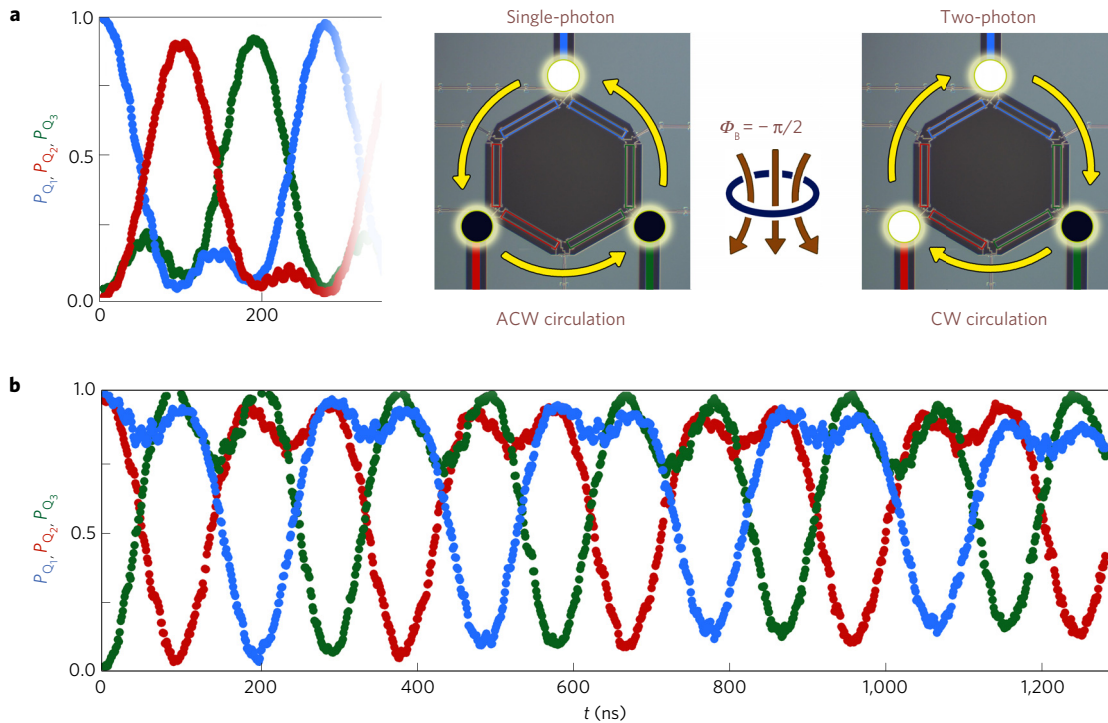


**Figure 3 | Signature of strong interaction. a**, The single-photon circulation data for  $\Phi_B = -\pi/2$ , which is shown in Fig. 2c, is partially shown for the ease of comparison with the two-photon data shown in **b**. **b**, At  $t=0$ , two photons are created and are occupying  $Q_1$  and  $Q_2$  sites. They are generated by applying a  $\pi$ -pulse to  $Q_1$  and  $Q_2$  and exciting them ( $\psi_0 = |110\rangle$ ). The parameters used, pulse sequence, and the measurements are similar to Fig. 2. While the single photon circulates in the anticlockwise direction, the photon-vacancy circulates in the clockwise direction. The counter circulation of the two-photon case compared with the single-photon case is the direct consequence of strong interactions in the system. In the absence of interactions, the direction of circulation would have been the same. These findings are schematically demonstrated in **a**. The yellow arrows indicate the direction of circulation of the single-photon or single-vacancy case, where photons and vacancies are depicted by bright and dark disks, respectively, and shown on top of the optical image of the circuit used.

Since  $\hat{I}_{\text{chiral}}$  flips sign under TRS, we expect that its ground-state expectation value will be zero whenever the Hamiltonian is TRS preserving, and non-zero otherwise. This equilibrium current is distinct from the commonly measured non-equilibrium particle imbalance<sup>42–44</sup>, as experimental measurement of  $\hat{I}_{\text{chiral}}$  requires access to the ground state.

To measure  $\langle \hat{I}_{\text{chiral}} \rangle$  in the single-photon manifold, initially we prepare  $\psi_0 = |100\rangle$ , followed by a ramp up of the Hamiltonian parameters to generate equation (2) for various  $\Phi_B$  values (olive colour, Fig. 4b). For preparing ground states in the two-photon manifold, we initially create  $\psi_0 = |110\rangle$  by exciting two qubits, followed by a similar ramp and measurements (maroon colour, Fig. 4b). Note that due to the large  $U/g$  ratio, the two-photon manifold with and without double occupancies are almost entirely separate. Because of the three-fold symmetry of the system, measuring the current operator between any pair of qubits, for example,  $\hat{I}_{Q_1 \rightarrow Q_2}$ , suffices for knowing  $\langle \hat{I}_{\text{chiral}} \rangle$ . The solid lines are from numerical computations assuming perfect adiabaticity. For a given  $\Phi_B$ , the measured  $\langle \hat{I}_{\text{chiral}} \rangle$  on single- and two-photon manifolds show almost exactly opposite values, indicating that photons and photon-vacancies have opposite chiralities. On both manifolds and away from the origin,  $\langle \hat{I}_{\text{chiral}} \rangle$  rather abruptly becomes non-zero with opposite values for  $\Phi_B > 0$  and  $\Phi_B < 0$ , showing a quantum transition. Additional interesting points are  $\Phi_B = \pm\pi$ , where  $\langle \hat{I}_{\text{chiral}} \rangle$  goes to zero on both one-photon and two-photon manifolds, and in contrast to  $\Phi_B = 0$ , the measured chiral current close to  $\Phi_B = \pm\pi$  is smooth.

The vanishing of  $\langle \hat{I}_{\text{chiral}} \rangle$  at  $\Phi_B = 0, \pm\pi$  can be understood by noticing that the Hamiltonian of the system is real at these points, and hence cannot break the TRS, whereas for other values it is irreducibly complex. Several features of the data can be understood

by computing the gap between the ground state and the first excited state (background colour of Fig. 4b). For  $\Phi_B = 0$ ,  $\langle \hat{I}_{\text{chiral}} \rangle$  is discontinuous, as the ground state is degenerate at  $\Phi_B = 0$  and any finite  $\Phi_B$  breaks this degeneracy and leads to chiral currents, effectively producing a first-order phase transition. On the other hand, for  $\Phi_B = \pm\pi$ , the ground state is not degenerate and there is a large gap to the excited states, and  $\langle \hat{I}_{\text{chiral}} \rangle$  must therefore smoothly cross zero as  $\Phi_B$  crosses  $\pm\pi$ . The origin of the oscillatory behaviour close to  $\Phi_B = 0$  is also due to gap closing, as a result of which the adiabatic ramps become incapable of providing the correct results.

### Towards realization of FQH states

Our experiment highlights the strengths of superconducting qubits for synthesizing many-body phases of quantum matter. The inherent simplicity of the coupling modulation method also played a key role in this first demonstration of synthetic gauge fields with superconducting qubits; frequently, synthetic gauge field proposals for superconducting circuits demand challenging new architectures and are susceptible to charge noise. The scheme we employed avoids these issues, can be generally applied for other applications<sup>34</sup>, and highlights a path forwards (see Supplementary Information for details) beyond these proof-of-principle experiments to the direct realization of FQH states. To realize FQH physics, the system must be large compared to the magnetic length  $l_B$  of the Hamiltonian. If we choose the Kapit-Mueller Hamiltonian<sup>28</sup> as a basis, a flux per plaquette  $\Phi_B = 1/3$  yields  $l_B = 0.69$ , which suggests an  $L \times L$  lattice with  $L \geq 6$  as an appropriate host for FQH physics. Further, a  $2 \times L$  ladder with nearest and next-nearest neighbour hopping can host a nearly exact Laughlin ground state that exhibits many of the properties of its  $L \times L$  parent state. These include a local excitation

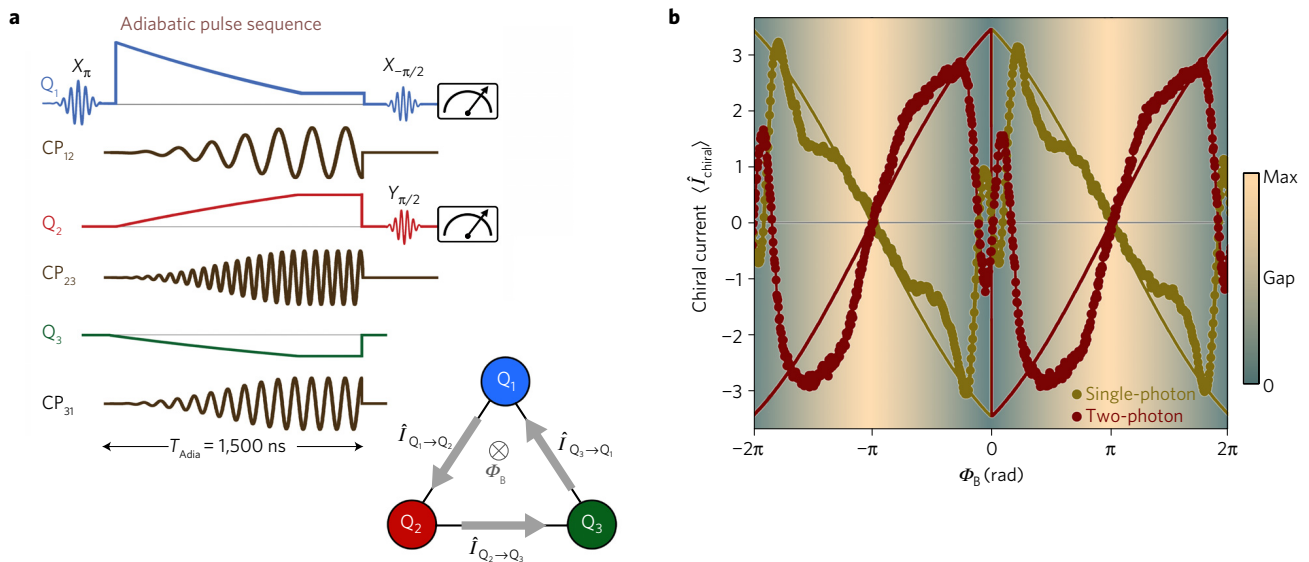


**Figure 4 | Chiral currents in the ground state.** **a**, The pulse sequence for adiabatically preparing the ground state of equation (2). For ground states in the single-photon manifold,  $Q_1$  is excited at  $t=0$  ( $\psi_0 = |100\rangle$ ), and in the two-photon manifold,  $Q_1$  and  $Q_2$  are excited ( $\psi_0 = |110\rangle$ ). To measure  $\hat{I}_{Q_1 \rightarrow Q_2}$  at the end of parameter ramping,  $Q_1$  and  $Q_2$  are rotated, allowing for measurements of  $\langle \sigma_{Q_1}^X \sigma_{Q_2}^Y \rangle$  and  $\langle \sigma_{Q_1}^Y \sigma_{Q_2}^X \rangle$ . **b**, The measured values of  $\langle \hat{I}_{\text{chiral}} \rangle$  in the single-photon (olive colour) or two-photon manifolds (maroon colour). The solid lines are computations for  $T_{\text{adia}} \rightarrow \infty$ . The energy gap of the Hamiltonian of the system (equation (2)) as a function of  $\Phi_B$  is numerically computed and is shown as the background of the data. The gap closes at  $\Phi_B = 0, \pm 2\pi$  and the ground state becomes degenerate (green regions). The maximum gap size is  $3g_0$ , which here is 12 MHz.

gap, fractionalized excitations and a topological degeneracy which manifests as charge density wave order in ladder systems<sup>45</sup>. For both host systems, the Laughlin ground state is resilient against local phase noise, and it can be prepared through adiabatic evolution or resonant sequential photon injection, or stabilized indefinitely through engineered dissipation<sup>46–48</sup>. Thus, simply increasing the size of our system provides a near-term experimental path for generating FQH states of light.

### Data availability

The data that support the plots within this Article and other findings of this study are available from the corresponding author upon reasonable request.

Received 31 May 2016; accepted 16 September 2016; published online 31 October 2016

### References

- Anderson, P. W. More is different. *Science* **177**, 393–396 (1972).
- Bloch, I., Dalibard, J. & Nascimbene, S. Quantum simulations with ultracold quantum gases. *Nat. Phys.* **8**, 267–276 (2012).
- Lin, Y.-J., Compton, R., Jimenez-Garcia, K., Porto, J. & Spielman, I. Synthetic magnetic fields for ultracold neutral atoms. *Nature* **462**, 628–632 (2009).
- Miyake, H., Siviloglou, G. A., Kennedy, C. J., Burton, W. C. & Ketterle, W. Realizing the Harper Hamiltonian with laser-assisted tunneling in optical lattices. *Phys. Rev. Lett.* **111**, 185302 (2013).
- Aidelsburger, M. *et al.* Realization of the Hofstadter Hamiltonian with ultracold atoms in optical lattices. *Phys. Rev. Lett.* **111**, 185301 (2013).
- Jotzu, G. *et al.* Experimental realization of the topological Haldane model with ultracold fermions. *Nature* **515**, 237–240 (2014).
- Hafezi, M., Mittal, S., Fan, J., Migdall, A. & Taylor, J. Imaging topological edge states in silicon photonics. *Nat. Photon.* **7**, 1001–1005 (2013).
- Rechtsman, M. *et al.* Photonic Floquet topological insulators. *Nature* **496**, 196–200 (2013).
- Lu, L., Joannopoulos, J. & Soljačić, M. Topological photonics. *Nat. Photon.* **8**, 821–829 (2014).
- Tzauang, L., Fang, K., Nussenzeve, P., Fan, S. & Lipson, M. Non-reciprocal phase shift induced by an effective magnetic flux for light. *Nat. Photon.* **8**, 701–705 (2014).
- Ningyuan, J., Owens, C., Sommer, A., Schuster, D. & Simon, J. Time- and site-resolved dynamics in a topological circuit. *Phys. Rev. X* **5**, 021031 (2015).
- Lu, D. *et al.* Chiral quantum walks. *Phys. Rev. A* **93**, 042302 (2016).
- Tsui, D. C., Stormer, H. L. & Gossard, A. C. Two-dimensional magnetotransport in the extreme quantum limit. *Phys. Rev. Lett.* **48**, 1559–1562 (1982).
- Laughlin, R. B. Anomalous quantum Hall effect: an incompressible quantum fluid with fractionally charged excitations. *Phys. Rev. Lett.* **50**, 1395–1398 (1983).
- Georgescu, I. M., Ashhab, S. & Nori, F. Quantum simulation. *Rev. Mod. Phys.* **86**, 153–185 (2014).
- Ignacio Cirac, J. & Zoller, P. Goals and opportunities in quantum simulation. *Nat. Phys.* **8**, 264–266 (2012).
- Aspuru-Guzik, A. & Walther, P. Photonic quantum simulators. *Nat. Phys.* **8**, 285–291 (2012).
- Houck, A. A., Tureci, H. E. & Koch, J. On-chip quantum simulation with superconducting circuits. *Nat. Phys.* **8**, 292–299 (2012).
- Buluta, I. & Nori, F. Quantum simulators. *Science* **326**, 108–111 (2009).
- Paredes, B., Zoller, P. & Cirac, J. I. Fractional quantum Hall regime of a gas of ultracold atoms. *Solid State Commun.* **127**, 155–162 (2003).
- Cho, J., Angelakis, D. G. & Bose, S. Fractional quantum Hall state in coupled cavities. *Phys. Rev. Lett.* **101**, 246809 (2008).
- Hayward, A. L. C., Martin, A. M. & Greentree, A. D. Fractional quantum Hall physics in Jaynes–Cummings–Hubbard lattices. *Phys. Rev. Lett.* **108**, 223602 (2012).
- Petrescu, A., Houck, A. A. & Le Hur, K. Anomalous Hall effects of light and chiral edge modes on the kagomé lattice. *Phys. Rev. A* **86**, 053804 (2012).
- Hafezi, M., Adhikari, P. & Taylor, J. M. Engineering three-body interaction and Pfaffian states in circuit QED systems. *Phys. Rev. B* **90**, 060503 (2014).
- Hafezi, M., Adhikari, P. & Taylor, J. M. Chemical potential for light by parametric coupling. *Phys. Rev. B* **92**, 174305 (2015).
- Nayak, C., Simon, S. H., Stern, A., Freedman, M. & Das Sarma, S. Non-Abelian anyons and topological quantum computation. *Rev. Mod. Phys.* **80**, 1083–1159 (2008).
- Bergholtz, E. J. & Liu, Z. Topological flat band models and fractional Chern insulators. *Int. J. Mod. Phys. B* **27**, 1330017 (2013).
- Kapit, E. & Mueller, E. Exact parent Hamiltonian for the quantum Hall states in a lattice. *Phys. Rev. Lett.* **105**, 215303 (2010).
- Jaksch, D. & Zoller, P. Creation of effective magnetic fields in optical lattices: the Hofstadter butterfly for cold neutral atoms. *New J. Phys.* **5**, 56 (2003).
- Hauke, P. *et al.* Non-Abelian gauge fields and topological insulators in shaken optical lattices. *Phys. Rev. Lett.* **109**, 145301 (2012).
- Koch, J., Houck, A. A., Le Hur, K. & Girvin, S. M. Time-reversal-symmetry breaking in circuit-QED-based photon lattices. *Phys. Rev. A* **82**, 043811 (2010).
- Nunnenkamp, A., Koch, J. & Girvin, S. M. Synthetic gauge fields and homodyne transmission in Jaynes–Cummings lattices. *New J. Phys.* **13**, 095008 (2011).

33. Fang, K., Yu, Z. & Fan, S. Realizing effective magnetic field for photons by controlling the phase of dynamic modulation. *Nat. Photon.* **6**, 782–787 (2012).
34. Kapit, E. Universal two-qubit interactions, measurement, and cooling for quantum simulation and computing. *Phys. Rev. A* **92**, 012302 (2015).
35. Chen, Y. *et al.* Qubit architecture with high coherence and fast tunable coupling. *Phys. Rev. Lett.* **113**, 220502 (2014).
36. Fang, K., Yu, Z. & Fan, S. Experimental demonstration of a photonic Aharonov–Bohm effect at radio frequencies. *Phys. Rev. B* **87**, 060301 (2013).
37. Estep, N. A., Sounas, D. L., Soric, J. & Alu, A. Magnetic-free non-reciprocity and isolation based on parametrically modulated coupled-resonator loops. *Nat. Phys.* **10**, 923–927 (2014).
38. Kerckhoff, J., Lalumiere, K., Chapman, B., Blais, A. & Lehnert, K. On-chip superconducting microwave circulator from synthetic rotation. *Phys. Rev. Appl.* **4**, 034002 (2015).
39. Raghu, S. & Haldane, F. D. M. Analogs of quantum-Hall-effect edge states in photonic crystals. *Phys. Rev. A* **78**, 033834 (2008).
40. Wang, Z., Chong, Y., Joannopoulos, J. & Soljačić, M. Observation of unidirectional backscattering-immune topological electromagnetic states. *Nature* **461**, 772–775 (2009).
41. Khanikaev, A. *et al.* Photonic topological insulators. *Nat. Mater.* **12**, 233–239 (2013).
42. Hugel, D. & Paredes, B. Chiral ladders and the edges of quantum Hall insulators. *Phys. Rev. A* **89**, 023619 (2014).
43. Kessler, S. & Marquardt, F. Single-site-resolved measurement of the current statistics in optical lattices. *Phys. Rev. A* **89**, 061601 (2014).
44. Atala, M. *et al.* Observation of chiral currents with ultracold atoms in bosonic ladders. *Nat. Phys.* **10**, 588–593 (2014).
45. Flavin, J. & Seidel, A. Abelian and non-abelian statistics in the coherent state representation. *Phys. Rev. X* **1**, 021015 (2011).
46. Kapit, E., Hafezi, M. & Simon, S. H. Induced self-stabilization in fractional quantum Hall states of light. *Phys. Rev. X* **4**, 031039 (2014).
47. Jin, J., Rossini, D., Fazio, R., Leib, M. & Hartmann, M. J. Photon solid phases in driven arrays of nonlinearly coupled cavities. *Phys. Rev. Lett.* **110**, 163605 (2013).
48. Tomadin, A. *et al.* Signatures of the superfluid-insulator phase transition in laser-driven dissipative nonlinear cavity arrays. *Phys. Rev. A* **81**, 061801 (2010).

### Acknowledgements

We acknowledge discussions with L. Lamata, A. Rahmani, E. Rico, M. Sanz and E. Solano. Devices were made at the UCSB Nanofab Facility, part of the NSF-funded NNIN, and the NanoStructures Cleanroom Facility.

### Author contributions

P.R., C.N. and A.M. performed the experiment. E.K. provided theoretical assistance. P.R. analysed the data, and with C.N. and E.K. co-wrote the manuscript and Supplementary Information. All of the UCSB and Google team members contributed to the experimental set-up. All authors contributed to the manuscript preparation.

### Additional information

Supplementary information is available in the [online version of the paper](#). Reprints and permissions information is available online at [www.nature.com/reprints](http://www.nature.com/reprints). Correspondence and requests for materials should be addressed to P.R.

### Competing financial interests

The authors declare no competing financial interests.